Intermetallics 139 (2021) 107366

Contents lists available at ScienceDirect

Intermetallics

journal homepage: www.elsevier.com/locate/intermet

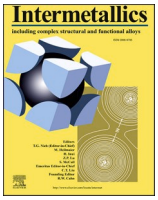

Consolidation and mechanical properties of $ZrCu_{39.85}Y_{2.37}Al_{1.8}$ bulk metallic glass obtained from gas-atomized powders by spark plasma sintering

M. Suárez [a,**], D. Fernández-González [a,*], L.A. Díaz [a], F. Diologent [b], L.F. Verdeja [c], A. Fernández [a]

[a] Centro de Investigación en Nanomateriales y Nanotecnología (CINN), Consejo Superior de Investigaciones Científicas (CSIC), Universidad de Oviedo (UO), Principado de Asturias (PA), Avda. de la Vega, 4-6, 33940, El Entrego, Asturias, Spain
[b] Richemont International SA, Recherche & Innovation, Rue de La Maladière, 71C, 2000, Neuchâtel, Switzerland
[c] Departamento de Ciencia de Los Materiales e Ingeniería Metalúrgica, Escuela de Minas, Energía y Materiales, Universidad de Oviedo, Calle Independencia, 33004, Oviedo, Asturias, Spain

ARTICLE INFO

Keywords:
Bulk metallic alloys
Zr–Cu alloy
Spark plasma sintering
Amorphous alloys
Densification
Sintering

ABSTRACT

This manuscript proposes subjecting gas-atomized powders of $ZrCu_{39.85}Y_{2.37}Al_{1.8}$ metallic glass to spark plasma sintering (SPS). This bulk metallic glass (BMG) sinters at a temperature between its crystallization (T_x) and glass transition (T_g) temperatures, found to be 457 °C and 368 °C, respectively, via Differential Scanning Calorimetry (DSC). Several samples were sintered at different temperatures within the mentioned range (380, 390, 400, 415 and 430 °C). Experimental results confirmed successful sintering of the BMG by SPS at 390 °C and a pressure of 35 MPa. Fully amorphous compacts with almost 100% relative density were sintered at this temperature, reaching Young's modulus, Vickers hardness and compression strength values of 64.7 GPa, 396 HV0.3 and 1174 MPa, respectively. Sintering at higher temperatures involved crystallization of the sample. Results suggest that $ZrCu_{39.85}Y_{2.37}Al_{1.8}$ metallic glass fabricated by SPS is a promising material for applications in different sectors, particularly jewelry, due to the wear resistance conferred by its hardness.

1. Introduction

The first Bulk Metallic Glasses (BMGs) appeared approximately 40 years ago. However, over the last decades, they have regained considerable interest due to their good mechanical strength, hardness, fracture toughness, corrosion resistance and yield strength [1–5]. The challenge with BMGs has always been to obtain a dense material while conserving the original amorphous structure. In this context, BMGs with low glass forming ability are seriously limited by their shape, size, and chemical composition [6]. Overcoming shape limitations involves machining in most cases, which can induce problems such as the crystallization of the already formed BMG. For this reason, the size of sintered BMGs has always been a challenge. Klement et al. manufactured the first metallic glasses (gold-silicon alloys) in 1960, which consisted only of thin ribbons [7]. Since then, BMG size has increased over the years: from 1 cm in the 90s [4,8,9] to samples of several centimeters, such as that obtained by Nishiyama et al. (80 mm in diameter, 85 mm in length and 3432 g of weight, in $Pd_{42.5}Cu_{30}Ni_{7.5}P_{20}$) around 2010 [10]. Currently, the maximum diameters reported for common BMGs are: Zr-based alloys, 20–73 mm; Ti-based alloys, 12 mm; Cu–Zr-based alloys, 30 mm; Mg-based alloys, 15 mm; Pd-based alloys, 80 mm [11].

Different densification methods have been proposed to obtain BMGs, including cold pressing [12], equal channel angular extrusion [13], hot pressing [14–17], injection [18], warm extrusion [16,17], injection mold casting, die mold casting, suction casting, squeeze casting, centrifugal casting, arc-melting casting [11,19], and spark plasma sintering (SPS). Among them, SPS or pulsed electric current sintering (PECS) has attracted special interest due to it allowing high-speed powder consolidation [20,21] and has, therefore, become a promising technique for BMG manufacturing [3]. Several types of BMGs have been manufactured via SPS, seeking applications in different fields: Cu-, Fe-, Ti-, Pb-, Zr-, Ni- and Al- based [2–4,6,22–35]. The main applications for BMGs include

* Corresponding author.
** Corresponding author.
E-mail addresses: m.suarez@cinn.es (M. Suárez), d.fernandez@cinn.es (D. Fernández-González).

https://doi.org/10.1016/j.intermet.2021.107366
Received 19 April 2021; Received in revised form 9 September 2021; Accepted 12 September 2021
Available online 20 September 2021

sports equipment, optical mirrors, communication equipment, magnetic applications, or engine components [36,37].

This manuscript focuses on Zr-based BMGs. This is a particular group of metallic glasses that has shown excellent mechanical properties, such as high specific strength, high hardness, good wear resistance, superplasticity in the supercooled liquid region, excellent physical and chemical properties (good anti-corrosion resistance, special expansion characteristics, special magnetic features, etc.) [38], and potential for biomedical applications due to its biocompatibility and non-cytotoxicity [39]. Therefore, a wide range of potential engineering applications has been proposed for Zr-based BMGs, which include sporting goods, energy penetrators, medical tools, ornaments, writing tools, and even promising applications in tribological and wear-resistant uses such as roller bearings [38]. BMGs from the Zr–Cu binary system have been widely studied alongside several microalloying elements: ZrCuAl (three adjacent eutectics in the Zr–Cu–Al alloy system [40]), ZrCuAlY ($Cu_{46}Zr_{42}Al_7Y_5$ [3]), ZrCuAgAl ($Zr_{100-x-y}(Cu_zAg_{1-z})_yAl_x$ (where x = 7–9 at.%, y = 38–50 at. % and z = 0.75–0.875), [41]; $Cu_{42-x}Zr_{42+x}Ag_8Al_8$ [42]), ZrCuAgTi ($Cu_{44.25}Ag_{14.75}Zr_{36}Ti_5$ [43]), ZrCuGdAl ($Cu_{46}Zr_{45}Al_7Gd_2$, [44]; $Cu_{46}Zr_{45}Al_7Gd_2$ [45]), ZrCuYAl ($Cu_{46}Zr_{47-x}Al_7Y_x$ ($0<x\leq 10$, in at. %) [46]), ZrCuFeAl ($Zr_{60}Cu_{30}Al_{10}$, $Zr_{60}Cu_{25}Al_{10}Fe_5$ and $Zr_{62.5}Cu_{22.5}Al_{10}Fe_5$, [47]; $Zr_{60}Cu_{25}Fe_5Al_{10}$ [48]), and other possible combinations. The aim of the present work was to obtain $ZrCu_{39.85}Y_{2.37}Al_{1.8}$ bulk metallic glass samples by spark plasma sintering gas-atomized powders with a dense and amorphous structure. This composition was chosen by Richemont International SA to be used in jewelry (watch gears) due to its wear resistance. Additionally, the proposed composition is close to that of the 920 °C eutectic in the Zr–Cu binary diagram, where yttrium and aluminum are added with the aim of avoiding allotropic transformations of zirconium and oxidation-nitriding problems during the manufacture of the amorphous material. The effect of the sintering temperature and its influence on the properties of the BMG are investigated in this manuscript.

2. Experimental procedures

$ZrCu_{39.85}Y_{2.37}Al_{1.8}$ metal alloy powders were used as the starting material. The synthesis of these metal alloy powders was carried out by atomizing the precursors using high gas pressure. Powders were supplied by Varinor (Richemont International SA).

First, $ZrCu_{39.85}Y_{2.37}Al_{1.8}$ powders were placed into a graphite die (50 mm inner diameter). A uniaxial pressure of 35 MPa was applied from the beginning of the cycle. A heating rate of 50 °C/min was employed up to the sintering temperature (380, 390, 400, 415 and 430 °C) and samples were held at that temperature for 5 min. Temperature was controlled by means of a thermocouple inserted into an opening in the mold wall. Finally, samples of 50 mm in diameter and 12 mm in thickness were obtained after sintering.

The microstructural characterization of $ZrCu_{39.85}Y_{2.37}Al_{1.8}$ glassy powders and sintered samples was performed by scanning electron microscopy (SEM) on a Hitachi TM3000 Scanning Electron Microscope equipped with a Bruker Quantax 70 Energy Dispersive X-ray Spectrometer. Fracture surfaces and polished surfaces of the sintered samples were subjected to SEM characterization after etching with 1%HF+1% HNO_3. Etching with hydrofluoric acid was performed to reveal the contours of the initially spherical powders, which in some cases can adopt a polygonal shape due to sintering mechanisms.

The crystallinity of the gas-atomized powders and sintered samples was investigated via X-Ray Diffraction (XRD) using a Bruker D8 Advance Powder X-ray Diffractometer with Cu-kα radiation (λ = 0.15406 nm). Working conditions included a copper anticathode cooled with water with an intensity of 40 mA and a voltage of 40 kV, a sweep between 5 and 70° with a step size of 0.03° and a step time of 0.5 s.

Thermal stabilities (glass transition, crystallization temperatures, etc.) were investigated by differential scanning calorimetry (DSC) using a TA Instruments SDT Q600 thermobalance. Analysis conditions included a heating rate of 5 °C/min, a temperature range of 30–800 °C, an argon atmosphere, and an alumina crucible.

The relative density of the sintered samples was determined via a geometric model using Eq. (1).

$$\rho\ (\%) = {}^{d}/_{d_{th}} \cdot 100 \tag{1}$$

Where d is the measured-apparent density and d_{th} is the theoretical density obtained by Helium pycnometry using an AccuPyc 1330 V2.04 N.

Vickers microhardness was determined using a Buehler Micromet 5103 microindentator. Measurements were made by applying loads of 300 gf, with an indentation time of 10 s, on samples polished down to a roughness of 1 μm. The applied load was worked out considering the Kick Law. Hardness was determined according to Eq. (2).

$$H_v = 1.853\ {}^{P}/_{d^2} \tag{2}$$

Where P stands for the applied load (in N) and d is the diagonal length of the indentation (in mm).

Uniaxial compression testing was conducted to investigate the mechanical properties of the BGM samples, using a universal mechanical testing machine (Instron, Model 8562). Quadrangular prisms with sides of 2.5 mm and heights of 4.9 mm were fixed on the testing platen. The compression strength was determined from the maximum load of the stress-strain curve, obtained from the load-displacement measurements by applying a 10 kN load cell and a strain rate of $1.7{\cdot}10^{-4}\ s^{-1}$. Stress (σ) was evaluated using Eq. (3). Tests were repeated three times (n = 3) for each sintering temperature.

$$\sigma = {}^{F}/_{A} \tag{3}$$

Where F is the compressive load and A is the cross sectional area of the specimen.

Finally, electrical conductivity was determined on both surfaces of the sintered disc using a Helmut Fischer GMBH Sigma Scope SMP350. The average value of 9 measurements was considered as a representative value of the electrical conductivity of the sample.

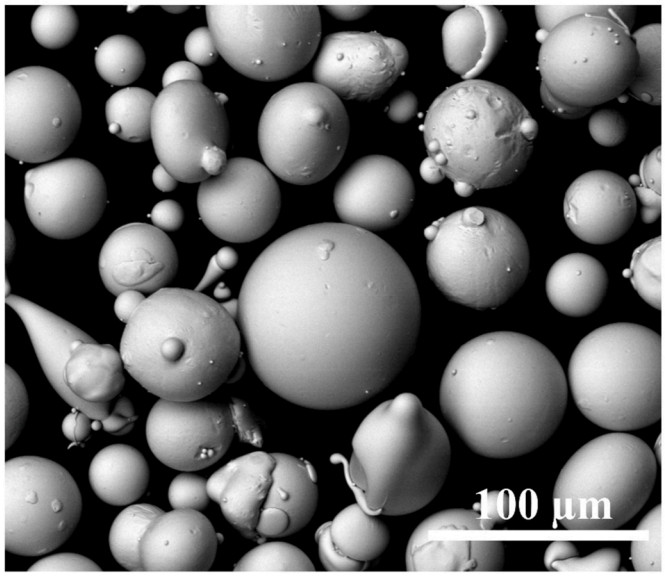

Fig. 1. SEM image of $ZrCu_{39.85}Y_{2.37}Al_{1.8}$ glassy powders, raw material.

3. Results

3.1. Gas-atomized powders

$ZrCu_{39.85}Y_{2.37}Al_{1.8}$ powders were characterized by SEM-EDX, XRD and DSC. The morphology of the initial powder is shown in Fig. 1. Particles are spherical in shape, displaying different sizes, as well as clean surfaces. Most of the particles are within the size range 20–100 μm (mean size (d_{50}) of 50 μm).

The thermodynamic parameters of the $ZrCu_{39.85}Y_{2.37}Al_{1.8}$ powders were determined via DSC, as shown in Fig. 2. The curve is typical for an amorphous material, with two peaks being observed. The first peak is located at around 368 °C (labeled T_g) and belongs to a second order transition corresponding to the glass transition temperature of the material. The second and exothermic peak, labeled T_x, at around 457 °C, is a first order transition and indicates that the material is beginning to crystallize. The temperature difference ΔT_x of the supercooled liquid region (SLR), described as the difference between the glass transition temperature (T_g) and the crystallization temperature (T_x), is approximately 90 °C. The SPS temperature should be within the given range, to avoid crystallization.

3.2. Influence of sintering temperature on densification

The aim of the present manuscript was to obtain a dense but amorphous material. Therefore, the sintering temperature had to be lower than the crystallization temperature (T_x, 457 °C), and within the range defined by this last temperature and the glass transition temperature (T_g, 368 °C). In this way, it is suitable for the densification of the powders to operate with low viscosity, to achieve an adequate viscous flow during sintering. Viscosity diminishes as temperature decreases, so it is usual to proceed at temperatures close to the glass transition temperature [6]. Moreover, temperature is a critical parameter for BMGs because crystallization can occur during heating, so sintering temperatures must not be excessively high. In this manner, X-ray diffraction patterns (at 415 and 430 °C) clearly reveal the crystalline phases formed during the sintering process: $Cu_{10}Zr_7$, CuZr and $Cu_{51}Zr_{14}$, as will later be indicated. These temperature values seem to be significantly lower than those obtained by DSC but, according to the literature [6], several reasons can explain this difference. The most relevant one is that the measured temperature may be significantly lower than the processing temperature, even if the thermocouple is close to the sample (the electric current may induce temperature differences and, at grain contact points, temperature may be significantly higher than that measured). So, SPS temperature is always below the glass transition temperature [3,6,27,28,49].

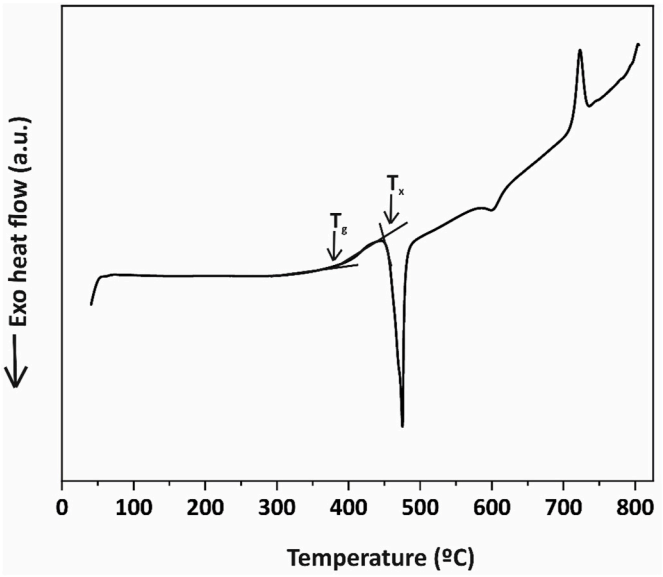

Fig. 2. DSC curve of the glassy powders.

A dilatometric analysis up to 600 °C was performed in the Spark Plasma apparatus to determine the sintering behavior of the $ZrCu_{39.85}Y_{2.37}Al_{1.8}$ powders. The linear shrinkage curve and its derivative are shown in Fig. 3. The material starts shrinking at 360 °C and the final sintering temperature is 470 °C. The maximum speed is reached at 430 °C. During the entire cycle, a pressure of 16 MPa was applied, and the heating rate was 50 °C/min. The dilatometric analysis determines the largest shrinkage velocity of the material, so that the different parameters, such as the final sintering temperature, the holding time, and the best moment for applying the pressure can be determined. As the dilatometric analysis is carried out at the minimum pressure admitted by the SPS equipment (16 MPa), all the processes take place at lower temperatures when sintering at greater pressure (35 MPa).

The apparent density of the samples (d) was determined by means of the geometric method for specimens sintered at different temperatures: 380, 390, 400, 415 and 430 °C. The theoretical density (d_{th}) of the BMG powders was obtained via Helium pycnometry, its value was found to be 6.9851 ± 0.0026 g/cm^3.

Table 1 shows the values of the apparent densities of the samples sintered by SPS as a function of the sintering temperature and the relative density calculated using equation (1). It is possible to confirm that almost 100% densification is reached by all the samples except for the sample sintered at 380 °C, which was not considered for further analysis due to the low densification achieved under those conditions. Samples sintered at 415 and 430 °C exhibit crystalline phases resulting from the transformation of the powders. These new crystalline phases imply a change in volume, thus leading to apparent densities greater to those of the original powders.

3.3. Microstructural analysis of the sintered samples

The XRD patterns obtained from the $ZrCu_{39.85}Y_{2.37}Al_{1.8}$ bulk alloy powders and the samples sintered at different temperatures are presented in Fig. 4. The initial BMG powders show a typical diffuse diffraction pattern corresponding to a glassy phase, where a broad band between 30 and 50° is observed. This indicates that the powder is completely amorphous. In the case of the sintered samples, it is possible to appreciate that the specimens sintered above 400 °C lose their amorphous behavior. At 400 °C, the peak corresponding to $Cu_{51}Zr_{14}$

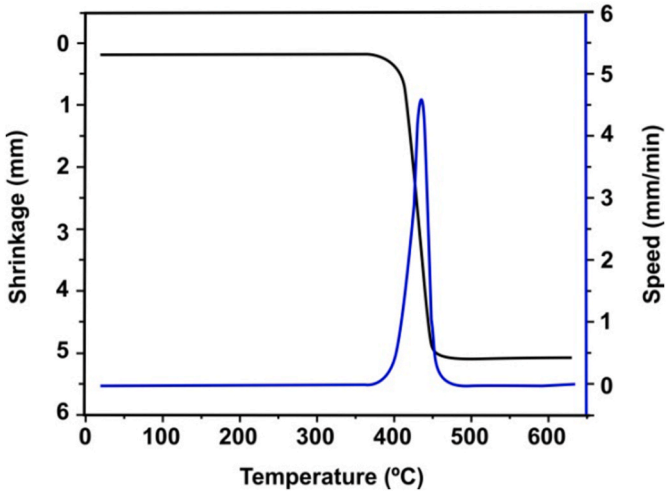

Fig. 3. Dilatometric linear shrinkage and speed curve for $ZrCu_{39.85}Y_{2.37}Al_{1.8}$ powders at 600 °C, applying a heating rate of 50 °C/min and a holding time of 1 min.

Table 1
Apparent density of samples sintered by SPS at different sintering temperatures and values of their relative densities.

Sintering temperature (°C)	Apparent density (g/cm^3)	ρ (%)
380	5.31	76
390	6.98	99.6
400	6.98	99.6
415	7.06	100
430	7.01	100

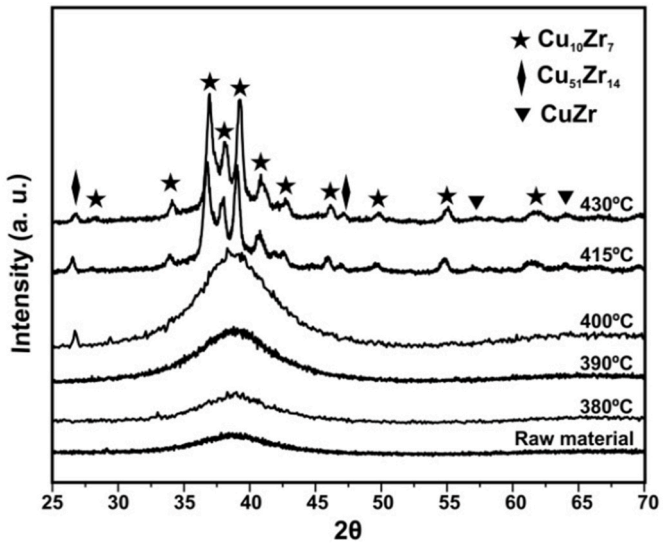

Fig. 4. XRD patterns of the product sintered at different temperatures. The pattern of the gas-atomized alloy powder is also shown for comparison purposes.

appears when 2θ is 26.5° alongside other incipient peaks in the 30–50° band, which indicates that the sample is not completely amorphous and explains some of the mechanical properties later determined. Specimens sintered at 415 and 430 °C exhibit a clearly crystalline behavior, since the diffraction peaks related to intermetallic phases are observed in the 2θ range of 30–50°, corresponding to $Cu_{10}Zr_7$, CuZr and $Cu_{51}Zr_{14}$.

It is important to notice that crystallization is strongly dependent on the sintering temperature, because the transition from amorphous state to crystalline state takes place within a narrow temperature range (90 °C) as was deduced from the DSC analysis. Anyway, it would make sense to think that an amorphous material would be obtained between 368 °C (glass transition temperature) and 457 °C (crystallization temperature). However, X-ray diffraction analyses indicate that an amorphous material is obtained only when T < 400 °C. Considering X-ray diffraction results and density values, the specimen sintered at 390 °C would be amorphous and almost 100% dense (99.6%). However, several pores/voids in the microstructure can be observed in Fig. 5a.

The microstructure of the sintered samples was observed by Scanning Electron Microscopy (Fig. 5a–d). Fig. 5a and b are SEM micrographs of the polished and etched surfaces of samples sintered at 390 °C and 400 °C, respectively. Analogous micrographs were obtained for samples sintered at 415 °C and 430 °C (Fig. 5c and d). The formation of necks between powder particles can be observed. The original morphology of the powder particles is maintained, though certain deformation of the powder particles can be observed. Small pores were identified at triple points (triangular shape) in the sample sintered at 390 °C. Pores were not identified in the samples sintered at 400, 415 and 430 °C.

3.4. Mechanical properties and mode of fracture

It is common for metallic materials with glassy structures to exhibit very high strength and hardness values, a relatively low Young's modulus and almost perfect elastic-plastic behavior upon room temperature deformation [50]. Compressive test and Vickers hardness measurements are typically used to evaluate the deformation and fracture mechanisms of BMG materials.

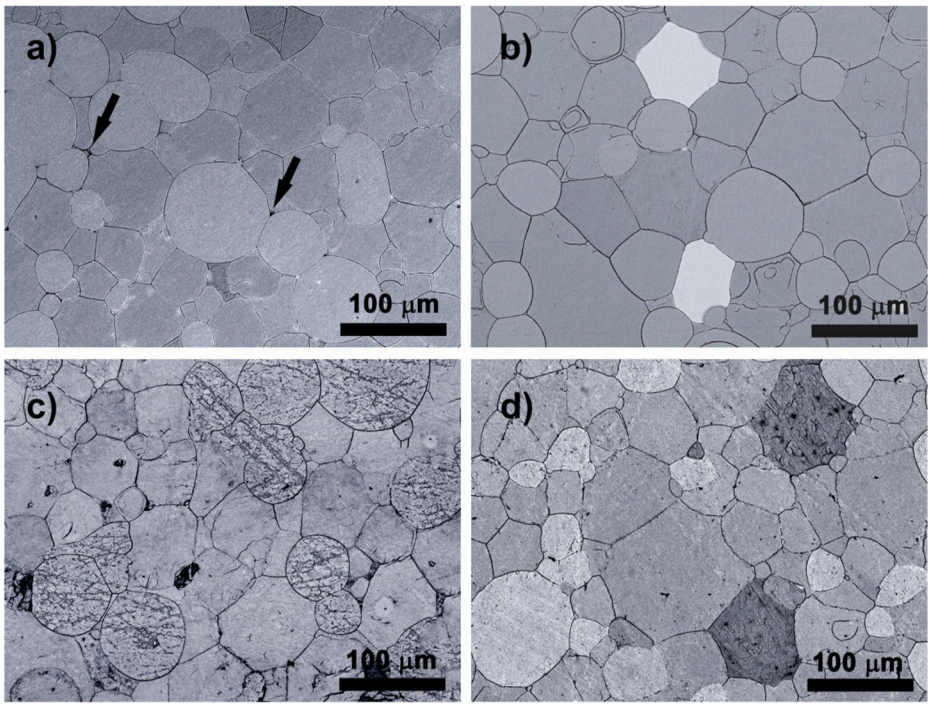

Fig. 5. SEM micrographs of the polished and etched surfaces of samples sintered at 390 °C (a), 400 °C (b), 415 °C (c) and 430 °C (d). The arrows in Fig. 5(a) reveal the pores (dark areas). In Fig. 5(b), crystalline grains appear in bright grey color (CuZr, $Cu_{51}Zr_{14}$ and $Cu_{10}Zr_7$).

The Vickers microhardness of the samples sintered at 390, 400, 415 and 430 °C was determined using equation (2). The average hardness values (10 indentations) of the samples sintered at the different temperatures are shown in Table 2. According to the literature [51], the increase in hardness with temperature could be attributed to (1) better inter-particle bonding, (2) higher density, (3) retained amorphous phase and (4) uniformly distributed hard intermetallic phases in the amorphous matrix. The slight decrease in hardness at 430 °C may be associated with the enhanced nucleation/growth of crystalline phases in the amorphous matrix [31]. At higher temperature, samples are denser, and hardness is greater due to the presence of crystalline particles [6].

Regarding the Young's modulus (E), Wang et al. [52] proposed a rough linear relationship between the Vickers hardness and the Young's modulus:

$$HV = \frac{0.06 \cdot E}{9.8} \rightarrow E = \frac{9.8 \cdot HV}{0.06} \quad (4)$$

The Young's modulus values determined using equation (4) are collected in Table 3. It is possible to see that the Young's modulus of the crystalline alloy is greater than that of the metallic glass. This is common for bulk metallic glasses [53].

The compressive properties of the sintered samples were evaluated by conventional compression testing. The stress-strain curves of the compression tests are represented in Fig. 6. It is possible to appreciate that the BMG's best compressive strength is reached when sintering at lower temperature, since the presence of crystalline particles can weaken the material [54]. The amorphous specimen (Fig. 6a) exhibits the greatest compressive strength value. The metallic glasses exhibit greater strain in the elastic domain than the crystalline alloys, but they do not show elastic behavior and barely present plastic deformation at room temperature due to the absence of dislocations or sliding planes, which represent an important factor in the plastic deformation of the crystalline alloys [53]. There is no plastic domain in either the amorphous or the crystalline samples. Therefore, the metallic glass exhibits greater mechanical strength than the crystalline alloy.

The fracture surfaces of the samples sintered at 390 °C and 400 °C were analyzed using Scanning Electron Microscopy. Both samples exhibit different fracture morphologies. At low temperature (390 °C, Fig. 7a), the powder particles retain their original spherical shape. Due to incomplete densification, the fracture surface of the sample exhibits an intergranular rupture mode, which reveals that the bond strength between grain interfaces is weak [55]. On the contrary, specimens sintered at 400 °C (Fig. 7b), which exhibit better densification and strong bonding, show cleavage breaking due to splitting along atomic planes. Metallic glass usually exhibits greater elastic deformation until fracture but, on the contrary, it does not show plastic deformation. This can be justified through the absence of both dislocations and sliding planes, which are important in the case of crystalline materials. Therefore, in the case of the sample sintered at 400 °C, which is at least partially crystalline, fracture occurs mostly along atomic planes and results in the morphology indicated in Fig. 7b, which is completely different from that seen in Fig. 7a, where fracture takes place at particle interfaces. However, plastic behavior is not observed, as can be deduced from Fig. 6.

Finally, the electrical conductivity was determined in different zones of the sintered discs. Results are collected in Table 4. It is possible to confirm that electrical conductivity is independent of the direction of the applied pressure and increases as the crystallinity of the sample increases. Samples exhibit electric conductivity comparable to that of other metals or alloys such as manganese or nichrome. The electrical conductivity of the alloy is lower than that of the crystalline alloy due to the random arrangement of the atoms, which prevents the smooth movement of electrons [53].

Table 2
Vickers hardness of the sintered samples.

Sintering temperature (°C)	Hardness (HV0.3)
390	396
400	479
415	493
430	482

Table 3
Young's modulus of the sintered samples.

Sintering temperature (°C)	Young's modulus (GPa)
390	64.68
400	78.24
415	80.52
430	78.73

4. Discussion

4.1. General considerations

Spark plasma sintering (SPS) is a newly developed rapid sintering technique that has great potential to produce amorphous materials or nanocrystalline materials in a short sintering time [20]. SPS is one of the novel techniques that is finding applications in different fields where fast heating rates are considered. Other potential competing techniques, although still not sufficiently developed, might be lasers, plasma, or concentrated solar energy, which are currently used in sintering but also in other different applications in the field of materials [56–61].

The GFA (glass-forming ability) of BMGs tends to increase when more components are added to the alloy [52]. This is called the "confusion principle", which implies that more components in the alloy system destabilize competing crystalline phases that may form during cooling [52]. This effect limits the tendency of the alloy to crystallize since it makes the melt more stable against crystalline phases. Inoue [62] proposed three rules for the formation of glass in multicomponent alloys: 1) multicomponent systems consisting of more than three elements, 2) a significant difference in atomic sizes with size ratios above about 12% among the three main constituent elements, and 3) negative heats of mixing among the three main constituent elements (although it has been recently reported that minor additions of elements that have a positive heat of mixing (PHM) with the constituent elements is also beneficial for improving GFA [63]). According to Inoue [62], alloys that satisfy these three empirical rules have atomic configurations in liquid state that favor glass formation in terms of thermodynamics, kinetics, and microstructure development. In this manuscript, Zr, Cu, Y and Al are the components of the system, their atomic diameters are $186 \cdot 1 \times 10^{-12}$ m, $140 \cdot 1 \times 10^{-12}$ m, $219 \cdot 1 \times 10^{-12}$ m and $184 \cdot 1 \times 10^{-12}$ m, respectively, and their heats of mixing are negative according to the tables in Ref. [64]. Therefore, the formation conditions for the proposed BMG are favored.

4.2. Densification mechanism

Bulk metallic glasses of a wide variety of alloy systems, including Zr-based, Cu-based or Ti-based alloys, among others, have been manufactured by sintering glassy powders. However, little has been reported about the densification mechanisms of metallic glass powders. Concerning this matter, the research of Liu et al. [65], Yang et al. [66] and Li et al. [67] provides details that could help understand the densification mechanism of BMGs. They describe the densification behavior of the glassy alloy using the instantaneous relative density, according to the variation in height of the consolidated specimen. In this way, the instantaneous relative density (ρ at time t) of the specimen is calculated using equation (5):

$$\rho = \rho_0 \cdot \left(\frac{h_0}{h}\right) \quad 5$$

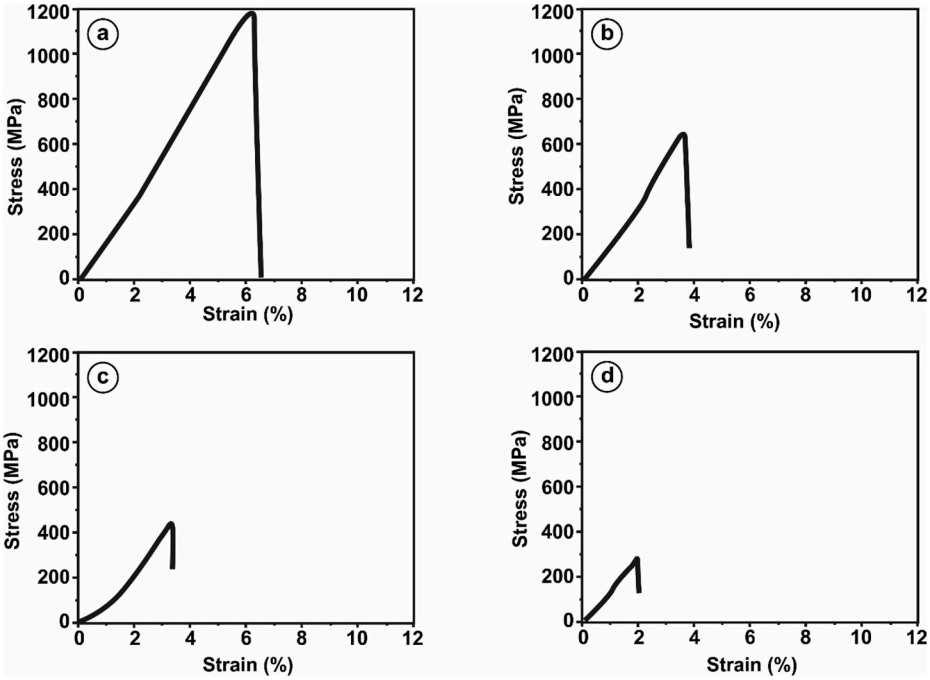

Fig. 6. Compressive stress-strain curve: 390 °C (a), 400 °C (b), 415 °C (c) and 430 °C (d).

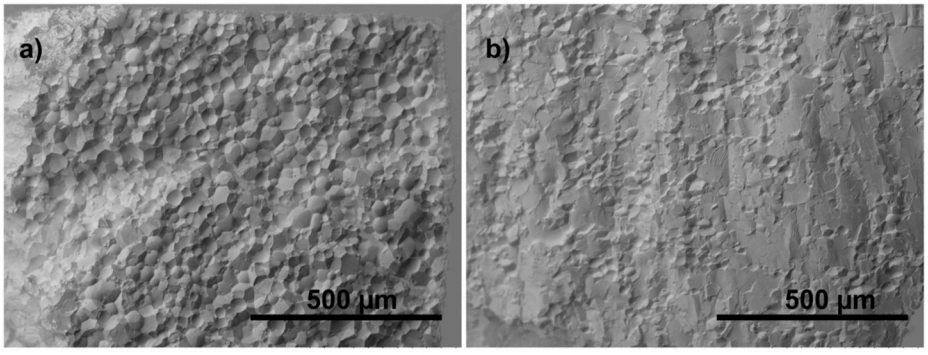

Fig. 7. SEM images of the fracture surfaces of the samples sintered by SPS at 390 °C (a) and 400 °C (b).

Table 4
Electrical conductivity data.

Sample	Electrical conductivity (MS/m)
390 °C	0.4595
400 °C	0.5277
415 °C	0.5578
430 °C	0.5321

where ρ_0 is the initial relative density, h_0 is the initial height of the specimen and h is the height at time t. The relative density as a function of the SPS temperature of the $ZrCu_{39.85}Y_{2.37}Al_{1.8}$ sample is represented in Fig. 8. It can be observed that the consolidated alloy has high relative density (>99.6%), as is quite common in BMGs.

Sintering of the BMG takes place via a solid-state sintering mechanism. In this way, particle bonding and densification are produced via the application of heat (and pressure) at temperatures well below the melting point (considering the Cu–Zr binary diagram, the minimum temperature required for the appearance of a liquid phase would be at least 920 °C (the eutectic point is close to the chemical composition chosen in this manuscript)). According to the literature [68,69] densification of BMGs by SPS could happen in two steps. At the beginning of

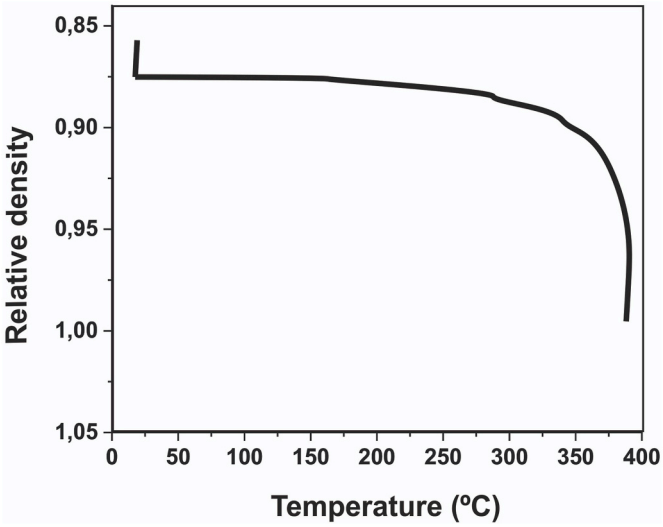

Fig. 8. Relative density as a function of the temperature during SPS of the MG $ZrCu_{39.85}Y_{2.37}Al_{1.8}$ powders.

the sintering process, cohesion between the particles is achieved and narrow necks are formed between them. Further densification should then occur during a second stage, which can be explained by the transition into the super-cooled liquid region of the material [70]. In this case, wider necks between the particles are formed, allowing a viscous flow but avoiding crystallization in the vicinity of the necks. The viscous flow of the amorphous powder has played a crucial role in densification with noticeable devitrification [51]. Viscosity decreases as sintering temperature increases, leading to increased viscous flow. When sintering temperature increases, crystalline particles can precipitate and grow through diffusion processes, as well as through powder particle bonding. In the case of BMGs sintered between 380 and 400 °C, a two-step process takes place. However, if temperature rises above 400 °C, crystallization happens.

Viscosity is important for densification [65–67]. The decreased viscosity of the BMG powder in the supercooled liquid region leads to a drastic reduction in porosity between the powder particles and promotes high densification rates.

Temperature is also an important factor in the densification of bulk metallic glasses. Too low sintering temperature induces an incomplete densification process; specimens are amorphous but not dense (i. e. porous), and their hardness is low. This is the case of the specimen sintered at 380 °C, its densification or relative density value is <80% and its properties are, for this reason, very poor. On the contrary, sintering at high temperatures leads to dense and hard specimens while crystalline behavior is increasingly lost. In this context, authors such as Zhang et al. [71] reported that annihilation of the free volume resulting from crystallization could increase the density. This is observed in samples sintered at or above 400 °C, which exhibit crystalline behavior and densification or relative density values of 100%. The nominal sintering temperature is selected below the glass transition temperature to avoid local crystallization, as represented in Fig. 9 [72,73]. Consequently, some colder positions inside the samples do not enter the supercooled liquid region, making full densification more difficult [3]. Hence, local overheating is a possibility that should be considered. Excessive deformation of the powder particles can cause them to become polyhedrons and stick together (the contact area is increased). The pulsed DC current of the SPS process directly generates joule heat inside the powder particles and enhances their densification [3,28,74]. Phenomena such as plasma formation and current density concentration occur, whereby local overheating takes place at the particle contacts. In this way, increasing the contact area reduces the difference in current density and temperature between the particle and the contact region, making the temperature field more uniform [72].

During sintering, different stages took place concurrent with the density increase: particle arrangement, localized deformation, viscous flow, and high temperature. Therefore, during the early stages of the sintering process, the size of the neck between the particles is very fine, leading to high current densities in their vicinity and, thus, to temperatures above T_x, responsible for the nanoprecipitation in these areas [28]. In this first stage, the heat generated at initial particle necks is extremely large when the neck is small, and its relaxation is very fast due to the high thermal diffusivity of metallic alloys. High intensity pulsed current is thus detrimental, and partial devitrification of the metallic glass is produced, together with the formation of high temperature phases and residual stresses resulting from the alternate cycles of heating and cooling. When the neck size is sufficient to limit the current density, there is homogeneous heating. In this context, there is an amorphous plastic flow of the particles, and it is possible to achieve complete densification [28].

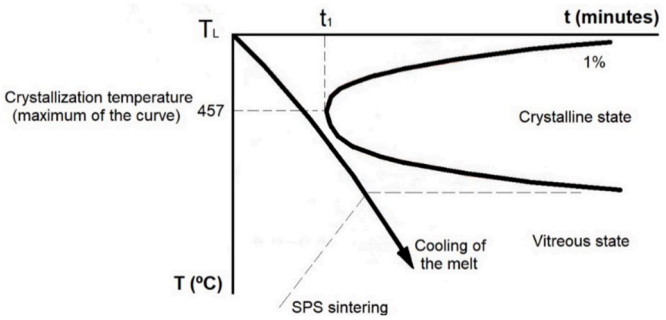

Fig. 9. Temperature-transformation-time curve.

4.3. Properties and selection of the BMG

As pointed out at the beginning of the manuscript, the composition of the BMG, $ZrCu_{39.85}Y_{2.37}Al_{1.8}$, was chosen by Richemont International SA, due to its wear resistance, to be used in jewelry (watch gears). The sintered product maintained its amorphous structure when sintered via SPS at 390 °C, reaching almost 100% densification (99.6%) in a supercooled liquid region of around 90 °C. The following properties were measured: Young's modulus = 64.7 GPa, Vickers hardness = 396 HV0.3 and compression strength = 1174 MPa.

Numerous Zr-based bulk metallic glasses have been studied by different researchers, as indicated in section 1.1, to be used in various applications. Their properties can be compared. In terms of Vickers hardness, the values obtained (396 HV0.3) are below others found in the literature for Zr–Cu–Al BMGs, such as: $Zr_{57}Cu_{20}Al_{10}Ni_8Ti_5$, 540 HV [28], or $Cu_{50}Zr_{45}Al_5$, 535 HV [6]. Regarding compression strength, the value obtained for the amorphous alloy (390 °C) in this research is 1174 MPa. Other metallic glasses exhibit similar values: Ding et al. [72] reached ~1200 MPa for Zr-based glass alloys, Chu et al. [3] ($Cu_{46}Zr_{42}Al_7Y_5$) achieved 1200–2000 MPa, Cardinal et al. [6] ($Cu_{50}Zr_{45}Al_5$) obtained 1600 MPa, and Nowak et al. [28] ($Zr_{57}Cu_{20}Al_{10}Ni_8Ti_5$) attained >1000 MPa. In all cases, a brittle fracture without a plastic domain is observed in the stress-strain curve. In our experiments, crystalline samples also show brittle behavior although their compressive strength is significantly lower, as observed by Ding et al. [72].

The values calculated in section 3.4 indicate that $ZrCu_{39.85}Y_{2.37}Al_{1.8}$ exhibits high strength and high hardness. The hardness of the sintered samples increases from 390 °C to 415 °C, which is attributable to an increase in the sintered density and the amount of devitrification with increasing sintering temperature, while it decreases at 430 °C due to precipitation/crystallization reactions and crystalline growth. However, the tendency of the strength is different, since by increasing the sintering temperature the compression fracture mode of the alloy transforms from a typical amorphous fracture to a crystalline brittle fracture.

Compared to other BMGs, including Zr-based BMGs, the densification of our alloy is almost complete. The supercooled liquid region is different, depending on the BMG (i. e., $Cu_{50}Zr_{45}Al_5$, 58 °C in Ref. [6]; $Cu_{46}Zr_{42}Al_7Y_5$, ~100 °C in Ref. [3]; $Zr_{57}Cu_{20}Al_{10}Ni_8Ti_5$, 60 °C in Ref. [28]). The pressure applied in our experiments was 35 MPa, reaching almost full densification when sintering at 390 °C, which indicates that it was sufficient to compensate the tensile stress between the particles during the shrinkage process. The pressures required to obtain 100% densification of other Zr-based BMGs are significantly higher: 90 MPa [6] for $Cu_{50}Zr_{45}Al_5$; 100, 200 and 300 MPa (>97.20%) [72] for different Zr-based BMGs; 600 MPa [3] for $Cu_{46}Zr_{42}Al_7Y_5$; 500 MPa [28] for $Zr_{57}Cu_{20}Al_{10}Ni_8Ti_5$.

Considering the above-mentioned properties and experimental conditions, bulk metallic glasses could find application in different fields. Inoue and Takeuchi [75] pointed out that there are BMGs undergoing practical use trials (or BMGs already in use) in companies in the fields of structural materials for machinery (due to their high strength) and optical precision (due to their high hardness). Wang et al. [52] indicate that bulk metallic glasses may be applied in the field of cutting materials. They also indicate that BMGs are attracting the interest of the fine jewelry industry as they can achieve an excellent surface finish alongside high performance characteristics and unique properties. Therefore,

considering the properties measured in this research, the $ZrCu_{39.85}Y_{2.37}Al_{1.8}$ BMG could be applied in the manufacture of gears for watches.

Ashby and co-authors were pioneers in the subject of material selection [76,77] since they proposed several relationships based on the mechanical properties of materials (properties of the most common materials are collected in Chapter 7 of [78]) for comparison purposes. The BMG obtained in this manuscript, $ZrCu_{39.85}Y_{2.37}Al_{1.8}$, exhibits mechanical properties like those of common metals, although the vitreous nature of this material limits its potential application as a structural material. However, its mechanical properties (hardness and compressive strength) are sufficient for functional applications as well as for other non-demanding applications. The main difficulty that arises when obtaining a BMG using SPS technology is the size of the sintered product, as well as its shape, since the former limits the potential applications and the latter requires additional machining operations.

5. Conclusions

A fully dense $ZrCu_{39.85}Y_{2.37}Al_{1.8}$ bulk metallic glass was successfully manufactured from gas-atomized glassy alloy powders using Spark Plasma Sintering. Material crystallization is strongly dependent on the sintering temperature since the transition from the amorphous to the crystalline structure takes place within a narrow temperature range. Therefore, sintering was carried out using SPS equipment at different temperatures within the range 380–415 °C, with a consolidation pressure of 35 MPa and a dwell time of 5 min. Sintered discs of 50 mm in diameter and 12 mm in thickness were subjected to a densification, microstructural and mechanical properties (hardness, Young's modulus, and compressive strength) study. The best results were obtained for the sample sintered at 390 °C, which resulted in an amorphous structure, almost 100% densification and the following properties: Young's modulus = 64.7 GPa, Vickers hardness = 396 HV0.3 and compression strength = 1174 MPa. Samples sintered at higher temperature also exhibited 100% densification and greater hardness, but they were partially or completely crystalline. On the contrary, samples sintered at 380 °C showed an amorphous structure and poor densification (≃75%), and therefore poor mechanical properties. $ZrCu_{39.85}Y_{2.37}Al_{1.8}$ bulk metallic glass was successfully sintered using SPS, and it was possible to verify that sintering temperature plays an important role when trying to obtain an amorphous alloy with adequate densification.

CRediT authorship contribution statement

M. Suárez: Conceptualization, Resources, Investigation, Writing – review & editing, Visualization. **D. Fernández-González:** Investigation, Writing – original draft, Writing – review & editing, Visualization. **L.A. Díaz:** Investigation, Visualization. **F. Diologent:** Conceptualization, Supervision. **L.F. Verdeja:** Writing – review & editing. **A. Fernández:** Conceptualization, Investigation, Supervision.

Declaration of competing interest

The authors declare that they have no known competing financial interests or personal relationships that could have appeared to influence the work reported in this paper.

Acknowledgements

The authors express their gratitude to Varinor SA for supplying the raw materials used during the research presented in this manuscript.

This research was also supported by a Juan de la Cierva Formación grant from the Spanish Ministry of Science and Innovation (MICINN) to Daniel Fernández-González (FJC2019-041139-I).

Authors are grateful to Ainhoa Macías San Miguel from the Nanomaterials and Nanotechnology Research Center (CINN) for providing excellent technical assistance.

References

[1] C. An-hui, X. Xiang, L. Yong, A. Wei-ke, Z. Guo-jun, L. Yun, L. Tie-lin, L. Xiao-song, Effect of consolidation parameters on mechanical properties of Cu-based bulk amorphous alloy consolidated by hot pressing, T. Nonferr. Metal. Soc. 22 (2012) 2032–2040, https://doi.org/10.1016/S1003-6326(11)61425-8.

[2] G. Xie, D.V. Louzguine-Luzgin, H. Kimura, A. Inoue, Nearly full density Ni52.5Nb10Zr15Ti12Pt7.5 bulk metallic glass obtained by spark plasma sintering of gas atomized powders, Appl. Phys. Lett. 90 (2007) 241902, https://doi.org/10.1063/1.2748102.

[3] Z.H. Chu, H. Kato, G.Q. Xie, G.Y. Yuan, W.J. Ding, A. Inoue, Consolidation and mechanical properties of Cu46Zr42Al7Y5 metallic glass by spark plasma sintering, J. Non-Cryst. Solids 358 (2012) 1263–1267, https://doi.org/10.1016/j.jnoncrysol.2012.02.027.

[4] P.P. Choi, J.S. Kim, O.T.H. Nguyen, H. D, Y.S. Kwon, J.C. Kwon, Kim, Al-La-Ni-Fe bulk metallic glasses produced by mechanical alloying and spark-plasma sintering, Mater. Sci. Eng. 449–451 (2007) 1119–1122, https://doi.org/10.1016/j.msea.2006.02.264.

[5] G. Xie, W. Zhang, D.V. Louzguine-Luzgin, H. Kimura, A. Inoue, Fabrication of porous Zr–Cu–Al–Ni bulk metallic glass by spark plasma sintering process, Scripta Mater. 55 (2006) 687–690, https://doi.org/10.1016/j.scriptamat.2006.06.034.

[6] S. Cardinal, J.M. Pelletier, J.C. Qiao, G. Bonnefont, G. Xie, Influence of spark plasma sintering parameters on the mechanical properties of $Cu_{50}Zr_{45}Al_5$ bulk metallic glass obtained using metallic glass powder, Mater. Sci. Eng. 677 (2016) 116–124, https://doi.org/10.1016/j.msea.2016.09.032.

[7] W. Klement, R.H. Willens, P. Duwez, Non-crystalline structure in solidified gold-silicon alloys, Nature 187 (1960) 869–875, https://doi.org/10.1038/187869b0.

[8] W.H. Wang, The elastic properties, elastic models and elastic perspectives of metallic glasses, Prog. Mater. Sci. 57 (2012) 487–656, https://doi.org/10.1016/j.pmatsci.2011.07.001.

[9] A. Inoue, T. Takeuchi, Recent development and application products of bulk glassy alloys, Acta Mater. 59 (2011) 2246–2267, https://doi.org/10.1016/j.actamat.2010.11.027.

[10] N. Nishiyama, K. Takenaka, H. Miura, N. Saidoh, Y. Zheng, A. Inoue, The world's biggest glassy alloy ever made, Intermetallics 30 (2012) 19–24, https://doi.org/10.1016/j.intermet.2012.03.020.

[11] T. Inoue, Bulk glassy alloys: historical development and current research, Eng. Lett. 1 (2015) 185–191, https://doi.org/10.15302/J-ENG-2015038.

[12] Y.B. Kim, D.H. Jang, H.K. Seok, K.Y. Kim, Fabrication of Fe-Si-B based amorphous powder cores by cold pressing and their magnetic properties, Mater. Sci. Eng. 449 (2007) 389–393, https://doi.org/10.1016/j.msea.2006.02.394. –451.

[13] J. Robertson, J.T. Kim, I. Karaman, K.T. Hartwaig, I.E. Anderson, Consolidation of amorphous copper-based powder by channel angular extrusion, J. Non-Cryst. Solids 317 (2003) 144–151, https://doi.org/10.1016/S0022-3093(02)01995-6.

[14] Y.B. Kim, H.M. Park, W.Y. Jeung, J.S. Bae, Vacuum hot pressing of gas-atomized Ni-Zr-Ti-Si-Sn amorphous powder, Mater. Sci. Eng. 368 (2004) 318–322, https://doi.org/10.1016/j.msea.2003.11.015.

[15] R. Wanatabe, N. Yodoshi, H. Kato, A. Kawasaki, Densification control in hot pressing of metallic glass powders, J. Jpn. Soc. Powd. Met. 55 (2008) 709–714, https://doi.org/10.2497/jjspm.55.709.

[16] N. Matsubara, K. Yanagimoto, A. Kawasaki, Sintering behavior of Ni-based metallic glass powder by precise hot pressing, J. Jpn. Soc. Powd. Met. 55 (2008) 715–719, https://doi.org/10.2497/jjspm.55.715.

[17] A.H. Cai, X. Xiong, Y. Liu, W.K. An, G.J. Zhou, Y. Luo, T.L. Li, X.S. Li, Effect of consolidation parameters on mechanical properties of Cu-based bulk amorphous alloy consolidated by hot pressing, T. Nonferr. Metal. Soc. 22 (2012), https://doi.org/10.1016/S1003-6326(11)61425-8, 2032–2040.

[18] C.K. Kim, C.Y. Son, D.J. Ha, T.S. Yoon, S. Lee, N.J. Kim, Microstructure and mechanical properties of powder injection molds products of Cu-based amorphous powders and Fe-based metamorphic powders, Mater. Sci. Eng. 476 (2008) 69–77, https://doi.org/10.1016/j.msea.2007.05.014.

[19] T. Inoue, F.L. Kong, S.L. Zhu, E. Shalaan, F.M. Al-Marzouki, Production methods and properties of engineering glassy alloys and composites, Intermetallics 58 (2015) 20–30, https://doi.org/10.1016/j.intermet.2014.11.001.

[20] M. Suárez, A. Fernández, J.L. Menéndez, R. Torrecillas, H.U. Kessel, J. Hennicke, R. Kirchner, T. Kessel, in: B. Ertug (Ed.), Challenges and Opportunities for Spark Plasma Sintering: A Key Technology for a New Generation of Materials, Sintering Applications, IntechOpen, London, UK, 2013, pp. 319–342, https://doi.org/10.5772/53706 (Chapter 13).

[21] J.P. Kelly, O.A. Graeve, Spark plasma sintering as an approach to manufacture bulk materials: feasibility and cost savings, JOM-J. Min. Met. Mat. S. 67 (2015) 29–33, https://doi.org/10.1007/s11837-014-1202-x.

[22] X. Li, A. Makino, H. Kato, A. Inoue, T. Kubota, $Fe_{76}Si_{9.6}B_{8.4}P_6$ glassy powder soft-magnetic cores with low core loss prepared by spark-plasma sintering, Mater. Sci. Eng., B 176 (2011) 1247–1250, https://doi.org/10.1016/j.mseb.2011.06.017.

[23] X.P. Li, M. Yan, H. Imai, K. Kondoh, J.Q. Wang, G.B. Schaffer, M. Qian, Fabrication of 10 mm diameter fully dense $Al_{86}Ni_6Y_{4.5}Co_2La_{1.5}$bulk metallic glass with high fracture strength, Mater. Sci. Eng. 568 (2013) 155–159, https://doi.org/10.1016/j.msea.2013.01.041.

[24] D.J. Wang, Y.J. Huang, J. Shen, Y.Q. Wu, H. Huang, J. Zou, Temperature influence on sintering with concurrent crystallization behavior in Ti-based metallic glassy powders, Mater. Sci. Eng. 527 (2010) 2662–2668, https://doi.org/10.1016/j.msea.2009.12.052.

[25] C.K. Kim, H.S. Lee, S.Y. Shin, J.C. Lee, D.H. Kim, S. Lee, Microstructure and mechanical properties of Cu-based bulk amorphous alloy billets fabricated by spark plasma sintering, Mater. Sci. Eng. 406 (2005) 293–299, https://doi.org/10.1016/j.msea.2005.06.043.

[26] T.S. Kim, J.Y. Ryu, J.K. Lee, J.C. Bae, Synthesis of Cu-base/Ni-base amorphous powder composites, Mater. Sci. Eng. 449 (2007) 804–808.

[27] G. Xie, M. Fukuhara, D.V. Louzguine-Luzgin, A. Inoue, Ultrasonic characteristics of porous $Zr_{55}Cu_{30}Al_{10}Ni_5$ bulk metallic glass fabricated by spark plasma sintering, Intermetallics 18 (2010) 2014–2018, https://doi.org/10.1016/j.intermet.2010.03.029.

[28] S. Nowak, L. Perrière, L. Dembinski, S. Tusseau-Nenez, Y. Champion, Approach of the spark plasma sintering mechanism in $Zr_{57}Cu_{20}Al_{10}Ni_8Ti_5$metallic glass, J. Alloys Compd. 509 (2011) 1011–1019, https://doi.org/10.1016/j.jallcom.2010.09.158.

[29] Z. Chu, G. Yuan, H. Kato, G. Xie, D. Yan, The study on interface and property of TiNb/Zr-based metallic glassy composite fabricated by SPS, J. Non-Cryst. Solids 426 (2015) 83–87, https://doi.org/10.1016/j.jnoncrysol.2015.07.008.

[30] G. Xie, D.V. Louzguine-Luzgin, A. Inoue, Formation and properties of two-phase bulk metallic glasses by spark plasma sintering, J. Alloys Compd. 5095 (2011) 5214–5218, https://doi.org/10.1016/j.jallcom.2010.10.007.

[31] S.P. Harimkar, S.R. Paital, A. Singh, R. Aalund, N.B. Dahotre, Microstructure and properties of spark plasma sintered Fe–Cr–Mo–Y–B–C bulk metallic glass, J. Non-Cryst. Solids 355 (2009) 2179–2182, https://doi.org/10.1016/j.jnoncrysol.2009.07.007.

[32] S.S. Deng, D.J. Wang, Q. Luo, Y.J. Huang, J. Shen, Spark plasma sintering of gas atomized AlNiYLaCo amorphous powders, Adv. Powder Technol. 26 (2015) 1696–1701, https://doi.org/10.1016/j.apt.2015.10.009.

[33] B. Zheng, D. Ashforf, Y. Zhou, S.N. Mathaudhu, J. Delplanque, E.J. Lavernia, Influence of mechanically milled powder and high pressure on spark plasma sintering of Mg–Cu–Gd metallic glasses, Acta Mater. 61 (2013) 4414–4428, https://doi.org/10.1016/j.actamat.2013.04.011.

[34] Y. Wu, H. Wang, H.H. Wu, Z.Y. Zhang, X.D. Hui, G.L. Chen, D. Ma, X.L. Wang, Z. P. Lu, Formation of Cu–Zr–Al bulk metallic glass composites with improved tensile properties, Acta Mater. 59 (2011) 2928–2936, https://doi.org/10.1016/j.actamat.2011.01.029.

[35] Z. Ning, W. Liang, M. Zhang, Z. Li, H. Sun, A. Liu, J. Sun, High tensile plasticity and strength of a CuZr-based bulk metallic glass composite, Mater. Des. 90 (2016) 145–150, https://doi.org/10.1016/j.matdes.2015.10.117.

[36] A. Inoue, X.M. Wang, W. Zhang, Developments and applications of bulk metallic glasses, Rev. Adv. Mater. Sci. 18 (2008) 1–9.

[37] M. Telford, The case for bulk metallic glass, Mater. Today 7 (2004) 36–43.

[38] M.Z. Ma, R.P. Liu, Y. Xiao, D.C. Lou, L. Liu, Q. Wang, W.K. Wang, Wear resistance of Zr-based bulk metallic glass applied in bearing rollers, Mater. Sci. Eng. 386 (2004) 326–330, https://doi.org/10.1016/j.msea.2004.07.054.

[39] Q. Chen, L. Liu, S. Zhang, The potential of Zr-based bulk metallic glasses as biomaterials, Front. Mater. Sci. China 4 (2010) 34–44, https://doi.org/10.1007/s11706-010-0004-5.

[40] D. Wang, H. Tan, Y. Li, Multiple maxima of GFA in three adjacent eutectics in Zr–Cu–Al alloy system – a metallographic way to pinpoint the best glass forming alloys, Acta Mater. 53 (2005) 2969–2979, https://doi.org/10.1016/j.actamat.2005.03.012.

[41] Q.K. Jiang, X.D. Wang, X.P. Niw, G.Q. Zhang, H. Ma, H.-J. Fecht, J. Bendnarcik, H. Franz, Y.G. Liu, Q.P. Cao, J.Z. Jiang, Zr–(Cu, Ag)–Al bulk metallic glasses, Acta Mater. 56 (2008) 1785–1796, https://doi.org/10.1016/j.actamat.2007.12.030.

[42] Q. Zhang, W. Zhang, A. Inoue, New Cu–Zr-based bulk metallic glasses with large diameters of up to 1.5 cm, Scripta Mater. 55 (2006) 711–713, https://doi.org/10.1016/j.scriptamat.2006.06.024.

[43] C. Dai, H. Guo, Y. Shen, Y. Li, E. Ma, J. Xu, A new centimeter–diameter Cu-based bulk metallic glass, Scripta Mater. 54 (2006) 1403–1408, https://doi.org/10.1016/j.scriptamat.2005.11.077.

[44] L. Yang, G. Guo, Structural origin of the high glass-forming ability in Gd doped bulk metallic glasses, Appl. Phys. Lett. 97 (2010), 091901, https://doi.org/10.1063/1.3485117.

[45] H.M. Fu, H. Wang, H.F. Zhang, Z.Q. Hu, The effect of Gd addition on the glass-forming ability of Cu–Zr–Al alloy, Scripta Mater. 55 (2006) 147–150, https://doi.org/10.1016/j.scriptamat.2006.03.052.

[46] D. Xu, G. Duan, W.L. Johnson, Unusual glass-forming ability of bulk amorphous alloys based on ordinary metal copper, Phys. Rev. Lett. 92 (2004) 245504.

[47] D.V. Louzguine-Luzgin, G. Xie, Q. Zhang, A. Inoue, Effect of Fe on the glass-forming ability, structure and devitrification behavior of Zr–Cu–Al bulk glass-forming alloys, Phil. Mag. 90 (2010) 1955–1968, https://doi.org/10.1080/14786430903571495.

[48] G.Q. Guo, L. Yang, Y. S, Structural investigation upon the high glass-forming ability in Fe-doped ZrCuAl multicomponent alloys, Intermetallics 71 (2016) 24–30, https://doi.org/10.1016/j.intermet.2015.11.008.

[49] S. Shin, T.-S. Kim, S.-K. Kang, The influence of spark plasma sintering temperature on the mechanical properties and corrosion resistance of $Zr_{65}Al_{10}Ni_{10}Cu_{15}$ metallic glass powder, Intermetallics 18 (2010) 2005–2008, https://doi.org/10.1016/j.intermet.2010.03.033.

[50] X.F. Pan, H. Zhang, Z.F. Zhang, M. Stoica, G. He, J. Eckert, Vickers hardness and compressive properties of bulk metallic glasses and nanostructure-dendrite composites, J. Mater. Res. 20 (2005) 2632–2638, https://doi.org/10.1557/JMR.2005.0328.

[51] A. Sahu, R.S. Maurya, T. Laha, Effect of sintering temperature on phase evolution of Al86Ni6Y4.5Co2La1.5 bulk amorphous composites synthesized via mechanical alloying and spark plasma sintering, Prog. Nat. Sci.-Mat. 29 (2019) 32–40, https://doi.org/10.1016/j.pnsc.2019.01.009.

[52] W.H. Wang, C. Dong, C.H. Shek, Bulk metallic glasses, Mater. Sci. Eng. R. 44 (2004) 45–89, https://doi.org/10.1016/j.mser.2004.03.001.

[53] S. Yamaura, W. Zhang, A. Inoue, Introduction to amorphous alloys and metallic glasses, in: Y. Setsuhara, T. Kamiya, S. Yamura (Eds.), Novel Structured Metallic and Inorganic Materials, Springer Nature Singapore Pte Ltd, Singapore, Singapore, 2019, pp. 3–22, https://doi.org/10.1007/978-981-13-7611-5_1.

[54] G. Wang, B. Jiang, X. Zhang, B. Zhou, L. Meng, Crystallization behavior and mechanical properties of Cu-based bulk metallic glass composites, Mater. Res. 22 (2019), e20190078, https://doi.org/10.1590/1980-5373-mr-2019-0078.

[55] Q. Chen, C.Y. Tang, K.C. Chan, L. Liu, Viscous flow during spark plasma sintering of Ti-based metallic glassy powders, J. Alloys Compd. 557 (2013) 98–101, https://doi.org/10.1016/j.jallcom.2012.12.129.

[56] D. Fernández-González, J. Prazuch, I. Ruiz-Bustinza, C. González-Gasca, J. Piñuela-Noval, L.F. Verdeja, Solar synthesis of calcium aluminates, Sol. Energy 171 (2018) 658–666, https://doi.org/10.1016/j.solener.2018.07.012.

[57] D. Fernández-González, J. Prazuch, I. Ruiz-Bustinza, C. González-Gasca, J. Piñuela-Noval, L.F. Verdeja, Iron metallurgy via concentrated solar energy, Metals 8 (2018), https://doi.org/10.3390/met8110873 art. 873.

[58] D. Fernández-González, I. Ruiz-Bustinza, C. González-Gasca, J. Piñuela-Noval, J. Mochón-Castaños, J. Sancho-Gorostiaga, L.F. Verdeja, Concentrated solar energy applications in materials science and metallurgy, Sol. Energy 170 (2018) 520–540, https://doi.org/10.1016/j.solener.2018.05.065.

[59] D. Fernández-González, J. Prazuch, I. Ruiz-Bustinza, C. González-Gasca, J. Piñuela-Noval, L.F. Verdeja, Transformations in the Mn-O-Si system using concentrated solar energy, Sol. Energy 184 (2018) 148–152, https://doi.org/10.1016/j.solener.2019.04.004.

[60] D. Fernández-González, J. Prazuch, I. Ruiz-Bustinza, C. González-Gasca, J. Piñuela-Noval, L.F. Verdeja, Transformations in the Si-O-Ca system: silicon-calcium via solar energy, Sol. Energy 181 (2018) 414–423, https://doi.org/10.1016/j.solener.2019.02.026.

[61] D. Fernández-González, J. Prazuch, I. Ruiz-Bustinza, C. González-Gasca, J. Piñuela-Noval, L.F. Verdeja, The treatment of Basic Oxygen Furnace (BOF) slag with concentrated solar energy, Sol. Energy 180 (2018) 372–382, https://doi.org/10.1016/j.solener.2019.01.055.

[62] A. Inoue, Stabilization of metallic supercooled liquid and bulk amorphous alloys, Acta Mater. 48 (2000) 279–306, https://doi.org/10.1016/S1359-6454(99)00300-6.

[63] D. Cao, Y. Wu, X.J. Liu, H. Wang, X.Z. Wang, Z.P. Lu, Enhancement of glass-forming ability and plasticity via alloying the elements having positive heat of mixing with Cu in $Cu_{48}Zr_{48}Al_4$ bulk metallic glass, J. Alloys Compd. 777 (2019) 382–391, https://doi.org/10.1016/j.jallcom.2018.10.396.

[64] A. Takeuchi, A. Inoue, Classification of bulk metallic glasses by atomic size difference, heat of mixing and period of constituent elements and its application to characterization of the main alloying element, Mater. Trans. 46 (2005) 2817–2829, https://doi.org/10.2320/matertrans.46.2817.

[65] L.H. Liu, C. Yang, Y.G. Yao, F. Wang, W.W. Zhang, Y. Long, Y.Y. Li, Densification mechanism of Ti-based metallic glass powders during spark plasma sintering process, Intermetallics 66 (2015) 1–7, https://doi.org/10.1016/j.intermet.2015.06.010.

[66] C. Yang, M.D. Zhu, X. Luo, L.H. Liu, W.W. Zhang, Y. Long, Z.Y. Xiao, Z.Q. Fu, L. C. Zhang, E. J Lavernia, Influence of powder properties on densification mechanism during spark plasma sintering, Scripta Mater. 139 (2017) 96–99, https://doi.org/10.1016/j.scriptamat.2017.06.034.

[67] X.X. Li, C. Yang, T. Chen, Z.Q. Fu, Y.Y. Li, O.M. Ivasishin, E.J. Lavernia, Determination of atomic diffusion coefficient via isochronal spark plasma sintering, Scripta Mater. 151 (2018) 47–52, https://doi.org/10.1016/j.scriptamat.2018.03.033.

[68] L. Perrière, M.-T. Thaï, S. Tusseau-Nenez, P. Ochin, M. Blétry, Y. Champion, Spark plasma sintering for metallic glasses processing, Rev. Métall. 109 (2012) 5–10, https://doi.org/10.1051/metal/2011074.

[69] L. Perrière, M.-T. Thai, S. Tusseau-Nenez, M. Blétry, Y. Champion, Spark plasma sintering of a Zr-based metallic glass, Adv. Eng. Mater. 13 (2011) 581–586, https://doi.org/10.1002/adem.201000334.

[70] P. Drescher, K. Witte, B. Yang, R. Steuer, O. Kessler, E. Burkel, C. Schick, H. Seitz, Composites of amorphous and nanocrystalline ZrCuAlNb bulk materials synthesized by spark plasma sintering, J. Alloys Compd. 667 (2016) 109–114, https://doi.org/10.1016/j.jallcom.2016.01.161.

[71] B. Zheng, D. Ashford, Y. Zhou, S.N. Mathaudhu, J.P. Delplanque, E.J. Lavernia, Influence of mechanically milled powder and high pressure on spark plasma sintering of Mg-Cu-Cd metallic glasses, Acta Mater. 61 (2013) 4414–4428, https://doi.org/10.1016/j.actamat.2013.04.011.

[72] L.F. Verdeja, J.P. Sancho, A. Ballester, R. González, Refractory and Ceramic Materials, Síntesis, Madrid, 2014.

[73] J.A. Pero-Sanz, M.J. Quintana, L.F. Verdeja, Solidification and Solid-State Transformations of Metals and Alloys, Elsevier, Boston, 2017.

[74] H. Ding, Z. Zhao, J. Jin, L. Deng, P. Gong, X. Wang, Densification mechanism of Zr-based bulk metallic glass prepared by two-step spark plasma sintering, J. Alloys Compd. 850 (2021) 156724, https://doi.org/10.1016/j.jallcom.2020.156724.

[75] A. Inoue, A. Takeuchi, Recent progress in bulk glassy alloys, Mater. Trans. 43 (2002) 1892–1906, https://doi.org/10.2320/matertrans.43.1892.

[76] A.L. Salimon, M.F. Ahsby, Y. Bréchet, A.L. Greer, Bulk metallic glasses: what are they good for? Mater. Sci. Eng. 375–377 (2004) 385–388, https://doi.org/10.1016/j.msea.2003.10.167.

[77] M.F. Ashby, A.L. Greer, Metallic glasses as structural materials, Scripta Mater. 54 (2006) 321–326, https://doi.org/10.1016/j.scriptamat.2005.09.051.

[78] J.A. Pero-Sanz, D. Fernández-González, L.F. Verdeja, Structural Materials: Properties and Selection, Springer International Publishing, Cham, 2019.